Neurochemical alterations of different cerebral regions in rats with myocardial ischemia-reperfusion injury based on proton nuclear magnetic spectroscopy analysis

Research Paper

Neurochemical alterations of different cerebral regions in rats with myocardial ischemia-reperfusion injury based on proton nuclear magnetic spectroscopy analysis

Mao-Hui Feng[1,2], Zhi-Xiao Li[3], Qian Wang[3], Anne Manyande[4], Yu-Juan Li[3], Shun-Yuan Li[5], Weiguo Xu[6], Hong-Bing Xiang[3]

[1]Department of Gastrointestinal Surgery, Zhongnan Hospital, Wuhan University, Wuhan, China
[2]The Clinical Medical Research Center of Peritoneal Cancer of Wuhan, Clinical Cancer Study Center of Hubei Province, Key Laboratory of Tumor Biological Behavior of Hubei Province, Wuhan, China
[3]Departments of Anesthesiology and Pain Medicine, Tongji Hospital of Tongji Medical College, Huazhong University of Science and Technology, Wuhan, China
[4]School of Human and Social Sciences, University of West London, London, UK
[5]Department of Anesthesiology, The First Affiliated Quanzhou Hospital of Fujian Medical University, Quanzhou, China
[6]Department of Orthopedics, Tongji Hospital of Tongji Medical College, Huazhong University of Science and Technology, Wuhan, China

Correspondence to: Hong-Bing Xiang, Weiguo Xu; **email:** hbxiang@tjh.tjmu.edu.cn, xuweiguo@tjh.tjmu.edu.cn
Keywords: myocardial ischemia-reperfusion injury, proton nuclear magnetic spectroscopy, thalamus, brainstem
Received: May 4, 2020 **Accepted:** October 27, 2020 **Published:** December 14, 2020

ABSTRACT

Background: Recent studies have demonstrated a complex and dynamic neural crosstalk between the heart and brain. A heart-brain interaction has been described regarding cardiac ischemia, but the cerebral metabolic mechanisms involved are unknown.

Methods: Male Sprague Dawley rats were randomly allocated into 2 groups: those receiving myocardial ischemia-reperfusion surgery (IR group, n =10) and surgical controls (Con group, n=10). These patterns of metabolic abnormalities in different brain regions were assessed using proton magnetic resonance spectroscopy (PMRS).

Results: Results assessed by echocardiography showed resultant cardiac dysfunction following heart ischemia-reperfusion. Compared with the control group, the altered metabolites in the IR group were taurine and choline, and differences mainly occurred in the thalamus and brainstem.

Conclusions: Alterations in cerebral taurine and choline are important findings offering new avenues to explore neuroprotective strategies for myocardial ischemia-reperfusion injury. These results provide preliminary evidence for understanding the cerebral metabolic process underlying myocardial ischemia-reperfusion injury in rats.

INTRODUCTION

Elucidating the connectivity and functionality of a particular heart-brain circuit is one of the most challenging research goals in cardiology and neuroscience. Various strategies have been developed to reveal brain neural networks [1–5]. Over the past decade there has been a renaissance in our understanding of heart-brain interaction; new technologies are beginning to provide key insights into metabolic crosstalk between the heart and brain in

response to internal and external cues [6, 7]. Myocardial ischemia-reperfusion injury (MIRI) is known to be associated with comorbid nociceptive disorders and increased mortality risk [8–12]. The mechanisms through which MIRI is linked to these negative outcomes remains unclear, in part due to limited knowledge of the pathophysiology of MIRI itself. Some clues to the pathophysiology of myocardial ischemia may be derived from its clinical features. Impairments associated with myocardial ischemia can be categorized into nociceptive [13, 14] and affective domains [15]. The first domain is associated with brain regions that most consistently involve the amygdala, thalamus, cortex, anterior singular cortex (ACC), periaqueductal gray and rostral ventromedial medulla (RVM) [15–19]. Structures more critically involved in MIRI, may include the brainstem [19, 20] and thalamic nucleus [7, 21].

Proton magnetic resonance spectroscopy (PMRS) has helped to elucidate the heart-brain interaction at the macro level. It is an important neuroimaging modality that can quantify the concentration of specific neurochemicals in the central nervous system including the spinal cord and brain. PMRS analysis of local metabolic changes in the brain provides a quick modality for evaluating the specific neuronal activity [22], which in turn is controlled by changes in cerebral blood flow [23]. Although the underlying neuro-metabolic coupling mechanisms are still not completely understood, PMRS has already become a valued tool to detect amino acid levels and thus, brain-wide metabolic networks mapping. In the current study, we used PMRS to examine the alterations of amino acid levels in different brain regions associated with myocardial IR injury reproduced by the intermittent occlusion of the left anterior descending coronary artery [9, 24–32].

RESULTS

Characteristics of myocardial ischemia tissues

With regard to rats in the IR group, we observed the development of ST-segment elevation and QRS complex changes on an electrocardiogram, and the obvious cyanotic change in the myocardium of the occluded area 30 min after cardiac ischemia. Otherwise, serum cardiac troponin cTnI in the IR group was significantly increased compared to the Con group 2h after reperfusion. These results verified the performance of successful occlusion of the left anterior descending coronary artery [33].

Cardiac function assessed by echocardiography

Average data of LVEF and LVFS were assessed by echocardiography in male SD rats. Rats subjected to MIRI exhibited significantly decreased cardiac contractile function measured by LVEF ($p < 0.01$) and LVFS ($p < 0.001$) at 2h after MIRI compared to surgical controls (Supplementary Figures 1, 2 and Supplementary Table 1), suggesting that MIRI induced cardiac dysfunction.

PMRS-based metabolic information at different brain regions

To address the concentrations of cerebral metabolites that may be related to myocardial IR injury, we selected four brain regions (medulla-pons, parietal cortex, striatum, and thalamus) to analyze the information on metabolites in the spectra [illustrated in Figures 1, 2, 3 and 4]. The average normalized spectra of the two groups and the basic metabolic information, including the metabolite name and the related chemical shift are shown in Figures 1, 2, 3 and 4.

Absolute metabolite concentrations differ markedly across rat brain regions after myocardial IR injury

We dissected 12 brain regions of two groups and employed PMRS spectra to examine the level of metabolites, including Cretine, Glycine, myo_Insitol, Taurine, Choline, Asparate, Glutamine, Glutamate, GABA, NAA, Alanine, and Lactate (Table 1 and Supplementary Table 2). We found that the level of metabolites was comparable across almost all different brain regions studied, including PC, OC, TC, MID, MED-PONs, STR, HP, and THA, except for PFC, OB, CE, and HYP (Table 1 and Supplementary Table 2). Interestingly, the PC, OC, TC, STR, HP, and THA in the IR group showed a higher level of Taurine compared to the Con group, whereas the level of Taurine in the other brain regions examined (including MID, MED-PONs) was not different between the IR group and Con group.

Changes in metabolic concentration of different cerebral regions after myocardial IR injury

In order to precisely assess cerebral changes after myocardial IR injury, absolute concentrations of all related metabolites were calculated and compared (Supplementary Table 2 and Figure 5). The average difference in normalized PMRS spectra of selected metabolites between the Con and IR groups are displayed in Figures 1, 2, 3 and 4.

Taurine is differentially expressed in various rat brain regions. In the case of Taurine, we observed higher levels in the PC ($p=0.018$), OC ($p=0.026$), TC ($p=0.025$), STR ($p=0.004$), HP ($p=0.009$), and THA ($p=0.032$) of the IR group compared to the Con group.

Otherwise, we found a higher concentration of Cretine (p=0.025) and Glycine (p=0.016) in the PC of the IR group compared to the Con group, respectively, and a higher concentration of NAA (p=0.047) in the TC of the IR group compared to Con group.

In the case of Choline, we observed lower levels in the MID (p=0.032), MED-PONs (p=0.046) of the IR group compared to the Con group, whereas higher levels in the THA (p=0.010) of the IR group compared to the Con group.

Simultaneously, we observed a higher concentration of GABA in the MED-PONs (p=0.043), glutamine in the STR (p=0.011), and myo_Insitol in the HP (p=0.025) of the IR group compared to the Con group.

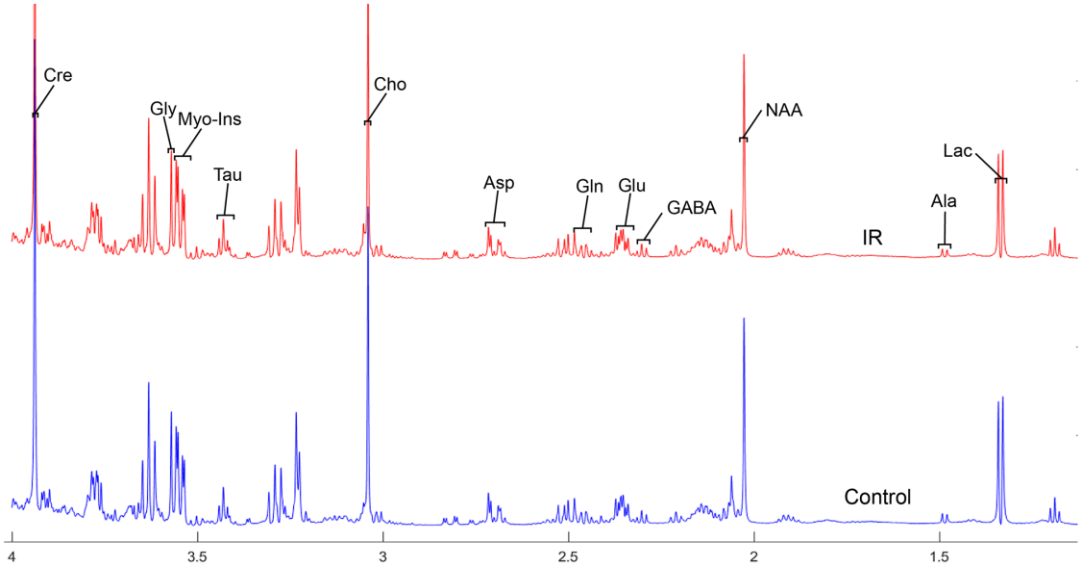

Figure 1. The normalized ^{1}H NMR spectra of extracts in medulla-pons after MIRI. Note: Lac, lactate; GABA, gamma-aminobutyric acid; NAA, N-acetylaspartate; Asp, aspartate; Glu, glutamine; Gln, Glutamate; Cre, creatinine; Cho, choline; Myo, Myo-inositol; Tau, taurine; Ala, alanine; Gly, glycine.

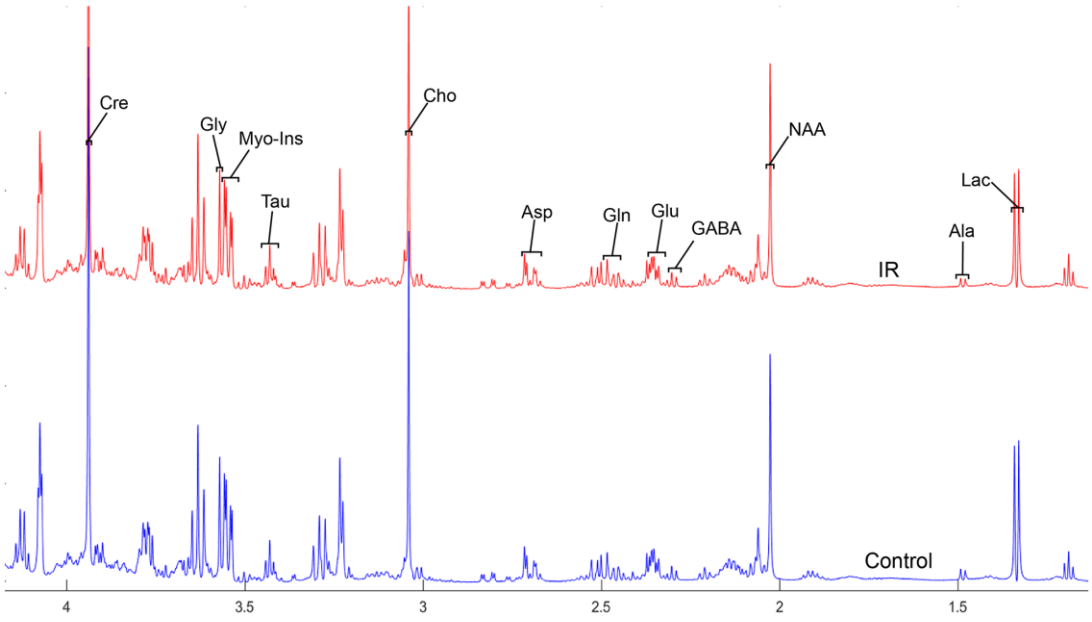

Figure 2. The normalized ^{1}H NMR spectra of extracts in the parietal cortex after MIRI.

Discriminant analysis between the two groups

Considering the vital function of metabolites including Cretine, Glycine, myo_Insitol, Taurine, Choline, Asparate, Glutamine, Glutamate, GABA, NAA, Alanine, and Lactate in different brain regions, metabolic changes in the medulla-pons, parietal cortex, striatum, and thalamus were further investigated (Figure 6). The Taurine changes in the FC are illustrated in Figure 7. Our results demonstrate that myocardial

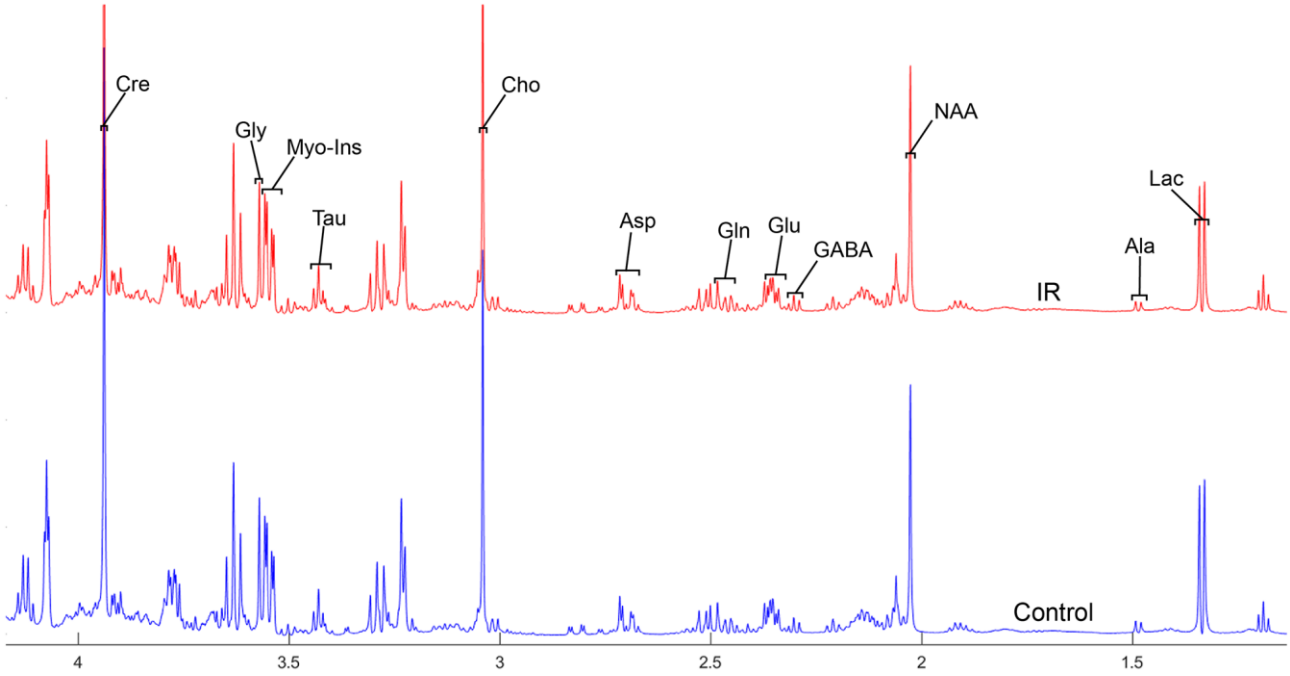

Figure 3. The normalized ^{1}H NMR spectra of extracts in the striatum after MIRI.

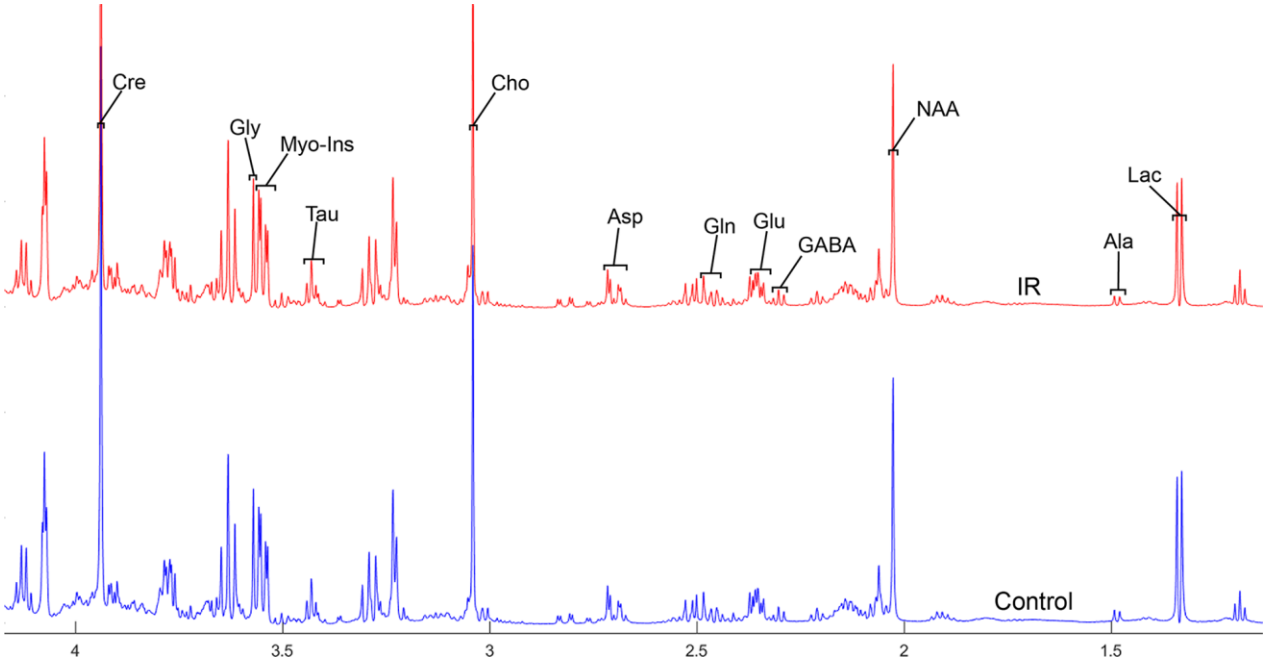

Figure 4. The normalized ^{1}H NMR spectra of extracts in the thalamus after MIRI.

Table 1. Various metabolites changes in different brain regions with MIRI in rats.

Brain regions	Metabolite	Variety
Medulla-Pons	**Cho**	32.1%↓ (P=0.046)
	GABA	16.1%↑(P=0.043)
Midbrain	**Cho**	28.6%↓ (P=0.032)
Hippocampus	**Myo-Ins**	6.3%↑(P=0.025)
	Tau	13.8%↑(P=0.009)
Striatum	**Tau**	14.1%↑(P=0.004)
	Gln	12.3%↑(P=0.011)
Thalamus	**Tau**	33.4%↑(P=0.032)
	Cho	40.5%↑(P=0.010)
Temporal cortex	**Tau**	20.7%↑(P=0.025)
	NAA	14.1%↑(P=0.047)
Parietal cortex	**Tau**	16.6%↑(P=0.018)
	Cre	8.1%↑(P=0.025)
	Gly	14.2%↑(P=0.016)
Occipital cortex	**Tau**	12.1%↑(P=0.026)

Note: The data were compared with control group. "↑"and "↓" indicates increase and decrease, respectively. Statistical analysis was performed by the Mann-Whitney test and P < 0.05 was considered significant difference. Cho, choline; GABA, gamma-aminobutyric acid; Myo-Ins, Myo- inositol; Tau, taurine; Gln, glutamine; Cre, creatinine; NAA, N-acetylaspartate; Gly, glycine.

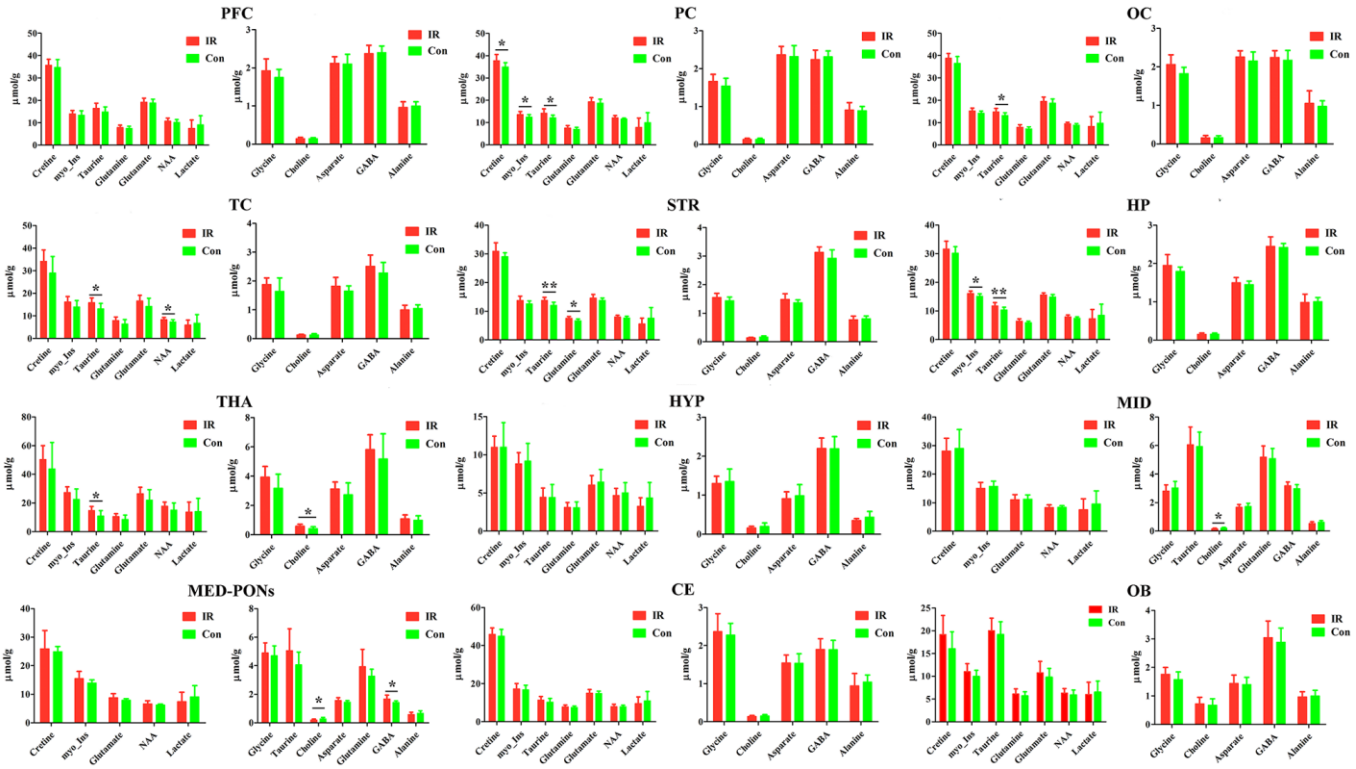

Figure 5. The concentration of identified metabolites in different brain regions in control (con) and ischemia reperfusion (IR) groups using the PMRS method. Data were presented as means ± SEM. Mann-Whitney test. *p< 0.05, **p<0.01. Note: FC, Prefrontal Cortex; PC, Parietal cortex; OC, Occipital cortex; TC, Temporal Cortex; STR, Striatum; HP, Hippocampus; HTA, Thalamus; HYP, Hypothalamus; MID, Midbrain; MED-PONs, Medulla-Pons; CE, Cerebellum; OB, Olfactory Bulbs; GABA, gamma amino acid butyric acid; NAA, N-acetyl aspartate.

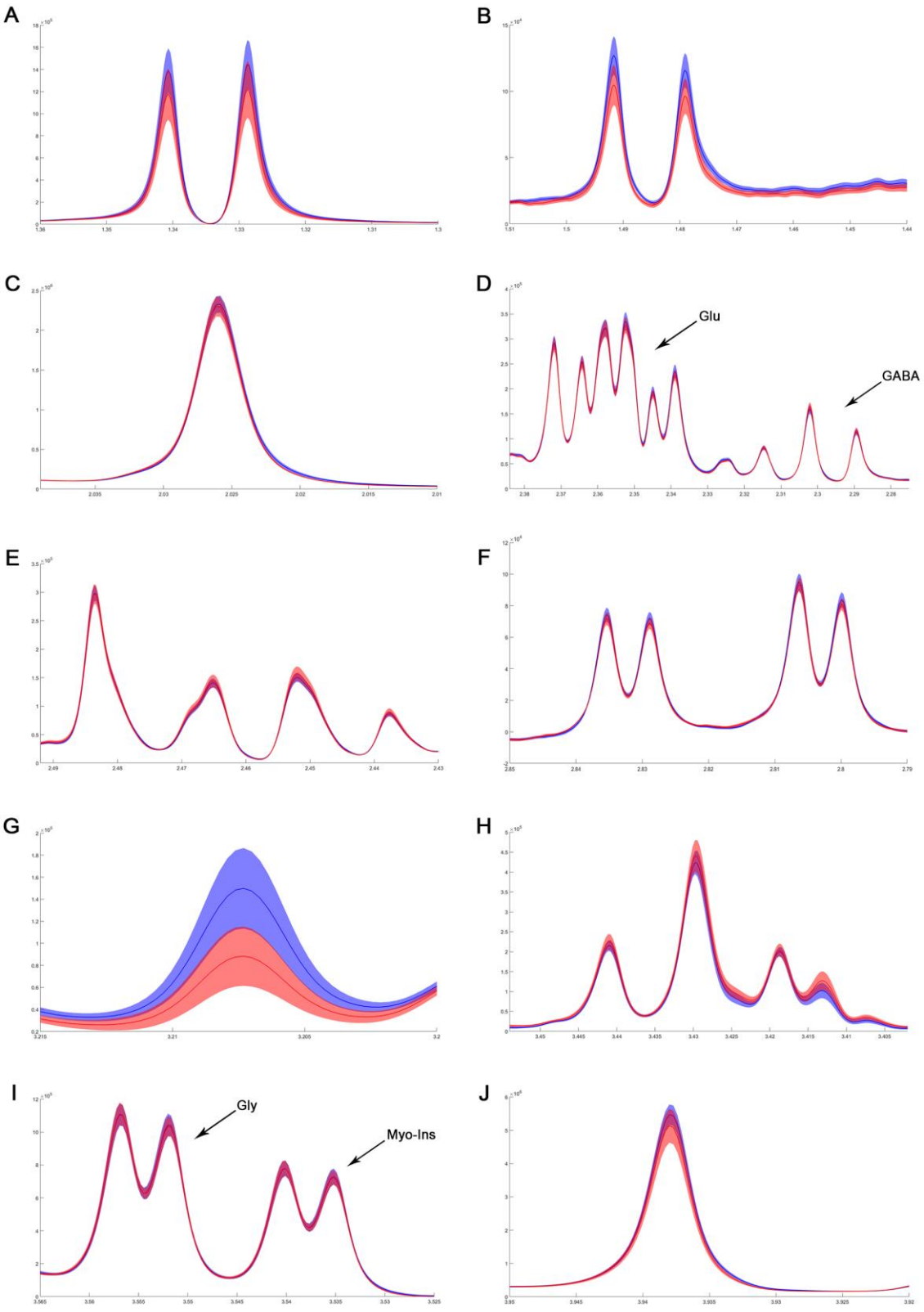

Figure 6. The difference in metabolites of normalized spectra in medulla-pons after MIRI. (**A**) Lactate; (**B**) Alanine; (**C**) N-acetylaspartate; (**D**) GABA and Glutamate; (**E**) Glutamine; (**F**) Aspartate; (**G**) Choline; (**H**) Taurine; (**I**) Myo-inositol and Glycine; (**J**) Creatinine. The spectral line and the width of its shadow represent mean and standard deviation, respectively. Control group: blue line with shadow around; IR group: red line with shadow around.

ischemia-reperfusion injury induced increase in Taurine levels in the Hippocampus, Occipital cortex, Striatum, Thalamus, and Temporal cortex.

DISCUSSION

Recently, significant efforts have been made to understand the alterations of amino acid levels in different brain regions and their contributions to specific metabolic disturbances of the disease [34–36]. The brain is a complex and dynamic metabolic structure for which functions are associated with the generation of energy activity in its targets [37]. Here, we aimed to understand the involvement of specific patterns of cerebral metabolites and glucose metabolism in different brain regions of animals with myocardial ischemia-reperfusion injury.

Compared to the control group, the rats in the IR group displayed a dramatic increase in the level of taurine in many brain regions including the PC, OC, TC, STR, HP, and THA, as well as a decrease in choline in the MID and MED-PONs but an increase in choline in the THA. It is well-known that taurine and creatine are neuroprotective metabolites [38–40]. Taurine is present in different brain regions and demonstrates an important inhibitory amino acid associated with extensive neuroprotective activities within the body [29, 41]. It has a functional role in osmoregulation in the brain under pathological conditions [38, 42, 43]. Jakaria et al. reported that taurine has potential therapeutic effects against different neurological disorders and protects against injuries and toxicities of the nervous system [39]. Wang et al. observed that rats with myocardial IR injury had higher concentration of taurine in the upper thoracic spinal cord, suggesting that

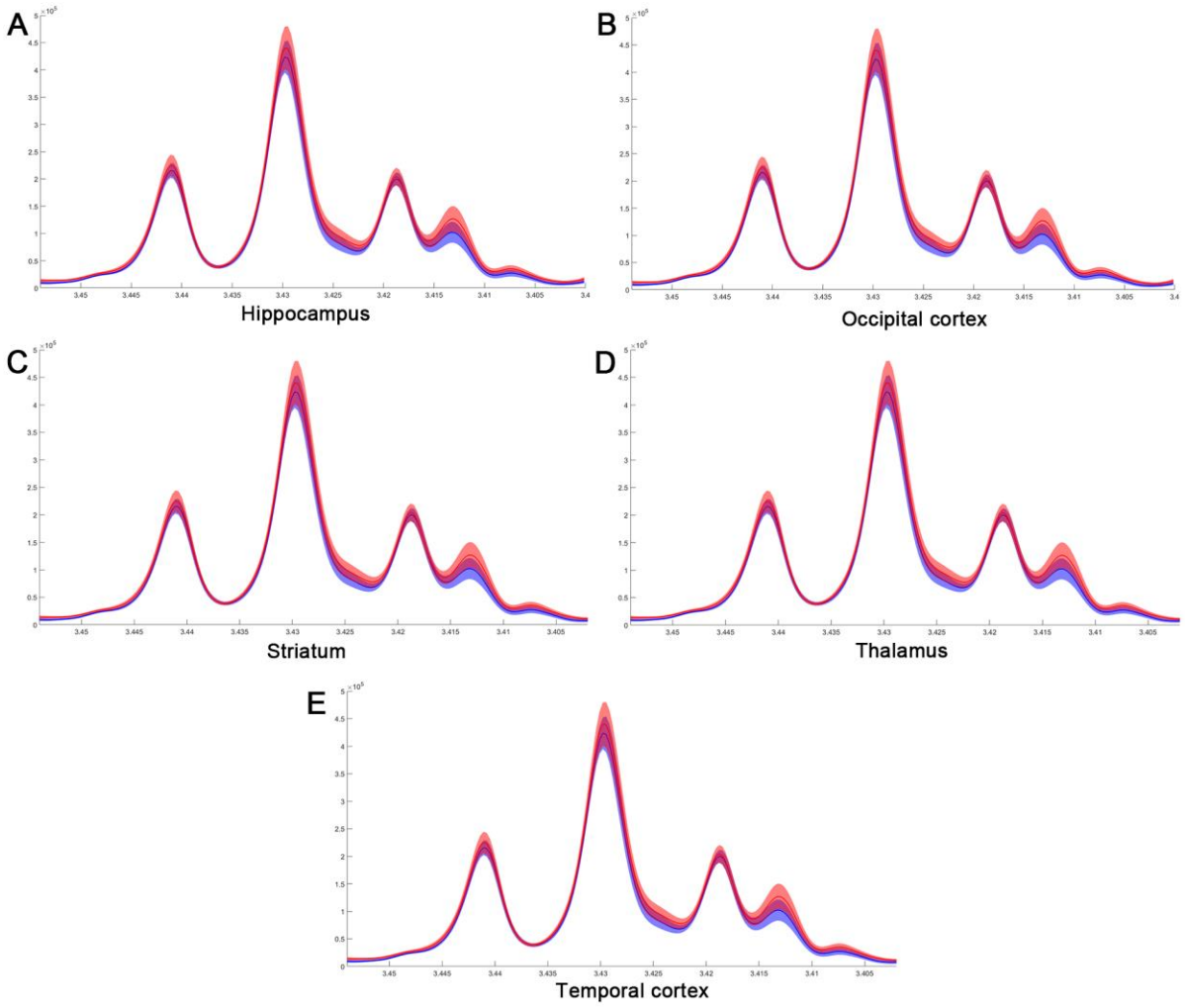

Figure 7. The difference in taurine of normalized spectra in different brain regions after MIRI. (**A**) Hippocampus; (**B**) Occipital cortex; (**C**) Striatum; (**D**) Thalamus; (**E**) Temporal cortex.

an alteration in spinal taurine associated with IR is involved in the effects of central regulation [8]. Consistent with these findings, our result indicates that IR increased cerebral concentrations of taurine in major brain regions, suggesting a critical role of taurine in the CNS during IR proceeding.

The thalamus (THA) is one of the most consistently implicated brain region in modulating cardiac functions. Previous studies have reported that acute myocardial ischemia induces increased neuronal activity in the parafascicular nucleus of the thalamus (PFT) [14, 44]. A study by Cheng and his colleagues demonstrated that cardioprotection was induced in a mouse model of chronic neuropathic pain via the anterior nucleus of the paraventricular thalamus [21]. Guo and Yuan showed that the discharge rate of PFT was markedly increased after coronary artery ischemia [44]. While Wang and Guo documented that the nociceptive-specific neuron in the PFT had a significant increase in the discharge rate following coronary ischemia [14], suggesting that there exists an important role for the PFT in regulating the nociception associated with acute myocardial ischemia. We observed an increase in taurine and choline of the THA in the IR group compared to the Con group. These results suggest an important role of the THA in the pathogenesis and regulation of myocardial IR injury.

In summary, we explored metabolic alterations of different cerebral regions in rats with myocardial ischemia-reperfusion injury by means of the PMRS. The metabolites that fluctuated most in the various cerebral regions were two critical amino-acids, taurine and choline. Our results provide preliminary evidence for understanding the cerebral metabolic process underlying myocardial ischemia-reperfusion injury in rats.

MATERIAL AND METHODS

Animal care

Animals were cared for according to the protection of vertebrate animals used for experimental purposes and institutional guidelines 86/609/CEE, November 24, 1986. The experiments were approved by the animal care committee of Tongji Medical College, Huazhong University of Science and Technology (No.TJ20150804) and were performed according to the ARRIVE (Animal Research: Reporting In Vivo Experiments) guidelines. Male Sprague Dawley (SD) rats weighing 250-300 g at the beginning of the experiment were housed at 22±1° C under a 12-hr light-dark cycle. They had free access to water and food until surgery. All procedures were conducted in an isolated quiet room to reduce variance.

Experimental design

Rats were randomly assigned to one of the two groups: those receiving myocardial ischemia-reperfusion surgery (IR group, n =10) and surgical controls (Con group, n=10). 2h after ischemia-reperfusion, all animals were prepared for the PMRS study.

Surgical procedure and myocardial IR injury model in rats

Myocardial IR surgeries were performed as previously described [9, 24, 25]. Briefly, prior to surgery, each rat was deeply anaesthetized and given atropine (0.25-0.3 ml of a 50 mg/ml solution intraperitoneally) to reduce salivation. After tracheal intubation, an invasive incision was made to expose the heart at the fourth intercostal space. The left anterior descending (LAD) coronary artery was then located and ligatured until myocardial ischemia occurred which was indicated by

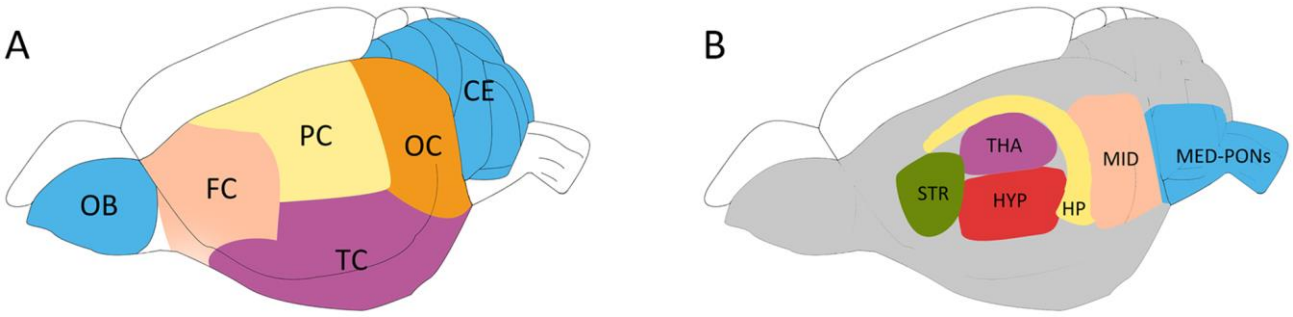

Figure 8. Schematic diagram showing the rat brain regions examined using proton NMR. Blue codes show the olfactory bulb (OB), cerebellum (CE) and cerebral cortical regions (**A**) and subcortical areas (**B**) studied. The OB and the cerebellum (CE) were first sampled, followed by the hippocampus (HP), the thalamus (THA) and the striatum (STR). The hypothalamus (HYP), the Midbrain (MID), and Medulla-Pons (MED-PONs) were discarded. The cerebral cortex tissues were coronally cut into four identical parts along the axial axis to represent the frontal cortex (FC), parietal cortex (PC), Temporal cortex (TC), and occipital cortex (OC).

visualizing a marked epicardial cyanosis. After 30 min of myocardial ischemia, the trap of the left anterior artery was opened. Reperfusion was allowed for 2 h. The surgical control group received the same surgical procedure, without any occlusion of the coronary artery and reperfusion. Rats in IR groups were monitored to confirm ST segment elevation during myocardial ischemia by the electrocardiogram. Cardiac Troponin I (cTnl) in two groups was measured 2h after reperfusion.

Echocardiography measurements

Cardiac function was assessed after 30 min of LAD occlusion and 2 h of reperfusion using transthoracic echocardiography measurements [26]. In brief, maintaining a steady-state sedation level with 1.5%–2.1% (v/v) isoflurane and 0.5 L/min 100% O_2 throughout the procedure, the anesthetized rats were placed in a supine position on top of a heating pad. After the pain reflex disappeared, a two-dimensional M-mode echocardiogram was used to obtain stable images via the parasternal long axis view for measuring left ventricular (LV) end-systolic diameter and LV end-diastolic diameter according to previously described data [27]. LV ejection fraction (EF) and LV fractional shortening (FS) were calculated. All data were analyzed by an observer who was blinded to the two groups.

Brain sample preparation for the PMRS study

To minimize the impact of post-mortem changes on cerebral metabolites [28], the anesthetized rat was microwaved using our previous method [29]. After euthanasia, the rat brain was quickly removed according to the Allen Brain Atlas [30] and dissected into 12 different regions (as indicated in Figure 8) [31]. Briefly, the olfactory bulb (OB) and the cerebellum (CE) were first sampled, followed by the hippocampus (HP), the thalamus (THA) and the striatum (STR). The hypothalamus (HYP), midbrain (MID) and medulla-pons (MED-PONs) were removed. After the entorhinal cortex was dissected, the remaining cerebral cortex tissue was coronally cut into four identical parts along the axial axis to represent the frontal cortex (FC), parietal cortex (PC), temporal cortex (TC), and occipital cortex (OC). These regional cerebral tissues were immediately weighed and stored at -80° C for further processing.

PMRS treatment and data processing

Protocols for cerebral tissue extraction, PMRS spectrum acquirement and PMRS data processing were the same as those described in our previous study [29, 30, 32]. Detailed methods are displayed in the Supplementary Materials. The 12 related peak areas were calculated separately (Figure 8).

Statistical analysis

Statistical data are shown as the mean ± standard error of the mean (SEM). Analysis was performed using GraphPad Prism 6.0. Comparisons between the two groups were performed using the Mann-Whitney U test. The P values of less than 0.05 were considered statistically significant.

AUTHOR CONTRIBUTIONS

MHF, ZXL and QW performed the animal experiment and analyzed the data. YJL and SYL prepared the first draft of the manuscript. MHF, WGX and HBX contributed to the study concept and design, and supervised the project. AM and HBX revised the manuscript.

ACKNOWLEDGMENTS

The authors would like to express their gratitude to Dr. Tao-Tao Liu (Department of Anesthesiology, Peking University Third Hospital) for his technical help.

CONFLICTS OF INTEREST

The authors declare no conflicts of interest.

FUNDING

This work was supported by grants from the National Natural Science Foundation of P.R. China (No. 81670240 and 81873467 to H.B. X, 81770283 and 82070302 to M.H. F), the Clinical Medical Research Center of Peritoneal Cancer of Wuhan (No.2015060911020462), the Research Foundation of Health and Family Planning Commission of Hubei Province (No.WJ2015MA010, No.WJ2017M249), the Natural Science Foundation of Hubei Province (No.2015CFA027), the National Natural Science Foundation of Hubei Province (No. 2016CFB625 to H.B. X), and the Medical innovation project in Fujian Province (No. 2017-CX-48 to S.Y. L).

REFERENCES

1. Gao X, Xu X, Hua X, Wang P, Li W, Li R. Group Similarity Constraint Functional Brain Network Estimation for Mild Cognitive Impairment Classification. Front Neurosci. 2020; 14:165. https://doi.org/10.3389/fnins.2020.00165 PMID:32210747

2. Li W, Zhang L, Qiao L, Shen D. Toward a better estimation of functional brain network for mild cognitive impairment identification: a transfer learning view. IEEE J Biomed Health Inform. 2020; 24:1160–68.

https://doi.org/10.1109/JBHI.2019.2934230
PMID:31403449

3. Chen D, Cheng X, Yang X, Zhang Y, He Z, Wang Q, Yao G, Liu X, Zeng S, Chen J, Xiang H. Mapping the brain-wide cholinergic neurons projecting to skeletal muscle in mice by high-throughput light sheet tomography. Neurosci Bull. 2020. [Epub ahead of print]. https://doi.org/10.1007/s12264-020-00552-0 PMID:32715391

4. Chen YL, He ZG, Wang Q, Xiang HB, Fan L, Xiong J. Specific patterns of spinal metabolite ratio underlying α-Me-5-HT-evoked pruritus compared with compound 48/80 based on proton nuclear magnetic resonance spectroscopy. Curr Med Sci. 2020; 40:761–66. https://doi.org/10.1007/s11596-020-2233-x PMID:32862388

5. Fan L, Xiang B, Xiong J, He Z, Xiang H. Use of viruses for interrogating viscera-specific projections in central nervous system. J Neurosci Methods. 2020; 341:108757. https://doi.org/10.1016/j.jneumeth.2020.108757 PMID:32371062

6. Mazzeo AT, Micalizzi A, Mascia L, Scicolone A, Siracusano L. Brain-heart crosstalk: the many faces of stress-related cardiomyopathy syndromes in anaesthesia and intensive care. Br J Anaesth. 2014; 112:803–15. https://doi.org/10.1093/bja/aeu046 PMID:24638232

7. Pan XC, Li ZX, Wu DZ, Li SY, Xiang HB, Song YT. Mapping changes of whole brain blood flow in rats with myocardial ischemia/reperfusion injury assessed by positron emission tomography. Curr Med Sci. 2019; 39:653–57. https://doi.org/10.1007/s11596-019-2087-2 PMID:31347004

8. Wang Q, Li ZX, Li YJ, Manyande A, Li SY, Feng MH, Wu DZ, Xiang HB. Alterations in amino acid levels and metabolite ratio of spinal cord in rat with myocardial ischemia-reperfusion injury by proton magnetic resonance spectroscopy. Am J Transl Res. 2019; 11:3101–08. PMID:31217879

9. Wang Q, Li ZX, Li YJ, He ZG, Chen YL, Feng MH, Li SY, Wu DZ, Xiang HB. Identification of lncRNA and mRNA expression profiles in rat spinal cords at various time-points following cardiac ischemia/reperfusion. Int J Mol Med. 2019; 43:2361–75. https://doi.org/10.3892/ijmm.2019.4151 PMID:30942426

10. Wang Q, He ZG, Li SY, Feng MH, Xiang HB. Application of animal and human PET in cardiac research. Am J Cardiovasc Dis. 2018; 8:24–30. PMID:30038843

11. Dong M, Yang Z, Fang H, Xiang J, Xu C, Zhou Y, Wu Q, Liu J. Aging attenuates cardiac contractility and affects therapeutic consequences for myocardial infarction. Aging Dis. 2020; 11:365–76. https://doi.org/10.14336/AD.2019.0522 PMID:32257547

12. Chen Q, Huang M, Wu J, Jiang Q, Zheng X. Exosomes isolated from the plasma of remote ischemic conditioning rats improved cardiac function and angiogenesis after myocardial infarction through targeting Hsp70. Aging (Albany NY). 2020; 12:3682–93. https://doi.org/10.18632/aging.102837 PMID:32074081

13. Huang C, Wang J, Wang N, Du F, Xiong W, Qian J, Zhong K, Cai A, Xu S, Huang J, Cheng X, He S, Zhang Y. Effect of myocardial ischemic preconditioning on ischemia-reperfusion stimulation-induced activation in rat thoracic spinal cord with functional MRI. Int J Cardiol. 2019; 285:59–64. https://doi.org/10.1016/j.ijcard.2019.03.025 PMID:30905517

14. Wang JP, Guo Z. Propofol suppresses activation of the nociception specific neuron in the parafascicular nucleus of the thalamus evoked by coronary artery occlusion in rats. Eur J Anaesthesiol. 2009; 26:60–65. https://doi.org/10.1097/EJA.0b013e328318c76a PMID:19122554

15. Gourine A, Gourine AV. Neural mechanisms of cardioprotection. Physiology (Bethesda). 2014; 29:133–40. https://doi.org/10.1152/physiol.00037.2013 PMID:24583769

16. Chen M, He ZG, Liu BW, Li ZX, Liu SG, Xiang HB. Parafascicular nucleus-heart neural crosstalk: implications for seizure-induced myocardial stunning. Epilepsy Behav. 2016; 63:135–37. https://doi.org/10.1016/j.yebeh.2016.06.036 PMID:27539366

17. Hao Y, Guan XH, Liu TT, He ZG, Xiang HB. Hypothesis: the central medial amygdala may be implicated in sudden unexpected death in epilepsy by melanocortinergic-sympathetic signaling. Epilepsy Behav. 2014; 41:30–32. https://doi.org/10.1016/j.yebeh.2014.09.017 PMID:25269692

18. Hao Y, Liu TT, He ZG, Wu W, Xiang HB. Hypothesis: CeM-PAG GABAergic circuits may be implicated in sudden unexpected death in epilepsy by melanocortinergic signaling. Epilepsy Behav. 2015; 50:25–28. https://doi.org/10.1016/j.yebeh.2015.04.070 PMID:26101104

19. Pickard JM, Burke N, Davidson SM, Yellon DM. Intrinsic cardiac ganglia and acetylcholine are important in the mechanism of ischaemic preconditioning. Basic Res Cardiol. 2017; 112:11. https://doi.org/10.1007/s00395-017-0601-x PMID:28091727

20. Mastitskaya S, Marina N, Gourine A, Gilbey MP, Spyer KM, Teschemacher AG, Kasparov S, Trapp S, Ackland GL, Gourine AV. Cardioprotection evoked by remote ischaemic preconditioning is critically dependent on the activity of vagal pre-ganglionic neurones. Cardiovasc Res. 2012; 95:487–94. https://doi.org/10.1093/cvr/cvs212 PMID:22739118

21. Cheng YF, Chang YT, Chen WH, Shih HC, Chen YH, Shyu BC, Chen CC. Cardioprotection induced in a mouse model of neuropathic pain via anterior nucleus of paraventricular thalamus. Nat Commun. 2017; 8:826. https://doi.org/10.1038/s41467-017-00891-z PMID:29018188

22. Wang SJ, Lirng JF, Fuh JL, Chen JJ. Reduction in hypothalamic 1H-MRS metabolite ratios in patients with cluster headache. J Neurol Neurosurg Psychiatry. 2006; 77:622–25. https://doi.org/10.1136/jnnp.2005.081836 PMID:16614022

23. Scherf T, Angenstein F. Hippocampal CA3 activation alleviates fMRI-BOLD responses in the rat prefrontal cortex induced by electrical VTA stimulation. PLoS One. 2017; 12:e0172926. https://doi.org/10.1371/journal.pone.0172926 PMID:28241047

24. Murry CE, Jennings RB, Reimer KA. Preconditioning with ischemia: a delay of lethal cell injury in ischemic myocardium. Circulation. 1986; 74:1124–36. https://doi.org/10.1161/01.cir.74.5.1124 PMID:3769170

25. Wang Q, He ZG, Li ZX, Li SY, Chen YL, Feng MH, Hong QX, Xiang HB. Bioinformatics analysis of gene expression profile data to screen key genes involved in cardiac ischemia-reperfusion injury. Int J Clin Exp Med. 2018; 11:4955–966.

26. Hedhli N, Huang Q, Kalinowski A, Palmeri M, Hu X, Russell RR, Russell KS. Endothelium-derived neuregulin protects the heart against ischemic injury. Circulation. 2011; 123:2254–62. https://doi.org/10.1161/CIRCULATIONAHA.110.991125 PMID:21555713

27. Li J, Qi D, Cheng H, Hu X, Miller EJ, Wu X, Russell KS, Mikush N, Zhang J, Xiao L, Sherwin RS, Young LH. Urocortin 2 autocrine/paracrine and pharmacologic effects to activate AMP-activated protein kinase in the heart. Proc Natl Acad Sci USA. 2013; 110:16133–38. https://doi.org/10.1073/pnas.1312775110 PMID:24043794

28. Shank RP, Aprison MH. Post mortem changes in the content and specific radioactivity of several amino acids in four areas of the rat brain. J Neurobiol. 1971; 2:145–51. https://doi.org/10.1002/neu.480020207 PMID:5160270

29. Liu T, He Z, Tian X, Kamal GM, Li Z, Liu Z, Liu H, Xu F, Wang J, Xiang H. Specific patterns of spinal metabolites underlying α-Me-5-HT-evoked pruritus compared with histamine and capsaicin assessed by proton nuclear magnetic resonance spectroscopy. Biochim Biophys Acta Mol Basis Dis. 2017; 1863:1222–30. https://doi.org/10.1016/j.bbadis.2017.03.011 PMID:28344131

30. Liu T, Li Z, He J, Yang N, Han D, Li Y, Tian X, Liu H, Manyande A, Xiang H, Xu F, Wang J, Guo X. Regional Metabolic Patterns of Abnormal Postoperative Behavioral Performance in Aged Mice Assessed by (1)H-NMR Dynamic Mapping Method. Neurosci Bull. 2020; 36:25–38. https://doi.org/10.1007/s12264-019-00414-4

31. Wang Y, Aun R, Tse FL. Brain uptake of dihydroergotamine after intravenous and nasal administration in the rat. Biopharm Drug Dispos. 1998; 19:571–75. https://doi.org/10.1002/(sici)1099-081x(199812)19:9<571::aid-bdd142>3.0.co;2-o PMID:9872338

32. Braissant O, Rackayová V, Pierzchala K, Grosse J, McLin VA, Cudalbu C. Longitudinal neurometabolic changes in the hippocampus of a rat model of chronic hepatic encephalopathy. J Hepatol. 2019; 71:505–15. https://doi.org/10.1016/j.jhep.2019.05.022 PMID:31173812

33. Huang CH, Lai CC, Yang AH, Chiang SC. Myocardial preconditioning reduces kidney injury and apoptosis induced by myocardial ischaemia and reperfusion. Eur J Cardiothorac Surg. 2015; 48:382–91. https://doi.org/10.1093/ejcts/ezu453 PMID:25475946

34. Wang J, Du H, Jiang L, Ma X, de Graaf RA, Behar KL, Mason GF. Oxidation of ethanol in the rat brain and effects associated with chronic ethanol exposure. Proc Natl Acad Sci USA. 2013; 110:14444–49. https://doi.org/10.1073/pnas.1306011110 PMID:23940368

35. Murray ME, Przybelski SA, Lesnick TG, Liesinger AM, Spychalla A, Zhang B, Gunter JL, Parisi JE, Boeve BF, Knopman DS, Petersen RC, Jack CR Jr, Dickson DW, Kantarci K. Early Alzheimer's disease neuropathology

detected by proton MR spectroscopy. J Neurosci. 2014; 34:16247–55.
https://doi.org/10.1523/JNEUROSCI.2027-14.2014
PMID:25471565

36. Maddock RJ, Casazza GA, Fernandez DH, Maddock MI. Acute modulation of cortical glutamate and GABA content by physical activity. J Neurosci. 2016; 36:2449–57.
https://doi.org/10.1523/JNEUROSCI.3455-15.2016
PMID:26911692

37. Fox MD, Snyder AZ, Vincent JL, Corbetta M, Van Essen DC, Raichle ME. The human brain is intrinsically organized into dynamic, anticorrelated functional networks. Proc Natl Acad Sci USA. 2005; 102:9673–78.
https://doi.org/10.1073/pnas.0504136102
PMID:15976020

38. Bruździak P, Panuszko A, Kaczkowska E, Piotrowski B, Daghir A, Demkowicz S, Stangret J. Taurine as a water structure breaker and protein stabilizer. Amino Acids. 2018; 50:125–40.
https://doi.org/10.1007/s00726-017-2499-x
PMID:29043510

39. Jakaria M, Azam S, Haque ME, Jo SH, Uddin MS, Kim IS, Choi DK. Taurine and its analogs in neurological disorders: focus on therapeutic potential and molecular mechanisms. Redox Biol. 2019; 24:101223.
https://doi.org/10.1016/j.redox.2019.101223
PMID:31141786

40. Lalande J, Halley H, Balayssac S, Gilard V, Déjean S, Martino R, Francés B, Lassalle JM, Malet-Martino M. 1H NMR metabolomic signatures in five brain regions of the AβPPswe Tg2576 mouse model of Alzheimer's disease at four ages. J Alzheimers Dis. 2014; 39:121–43.
https://doi.org/10.3233/JAD-130023 PMID:24145382

41. Madura JD, Lombardini JB, Briggs JM, Minor DL, Wierzbicki A. Physical and structural properties of taurine and taurine analogues. Amino Acids. 1997; 13:131–39.
https://doi.org/10.1007/BF01373211

42. Wade JV, Olson JP, Samson FE, Nelson SR, Pazdernik TL. A possible role for taurine in osmoregulation within the brain. J Neurochem. 1988; 51:740–45.
https://doi.org/10.1111/j.1471-4159.1988.tb01807.x
PMID:3411323

43. Taylor DL, Davies SE, Obrenovitch TP, Doheny MH, Patsalos PN, Clark JB, Symon L. Investigation into the role of N-acetylaspartate in cerebral osmoregulation. J Neurochem. 1995; 65:275–81.
https://doi.org/10.1046/j.1471-4159.1995.65010275.x
PMID:7790871

44. Guo Z, Yuan DJ. Midazolam inhibits cardiac nociception evoked by coronary artery occlusion in rats. Eur J Anaesthesiol. 2008; 25:479–84.
https://doi.org/10.1017/S0265021508003815
PMID:18289449

SUPPLEMENTARY MATERIALS

Supplementary Information

The protocol for tissue extraction was the same as that in our previous study [1]. Briefly, HCl/methanol (0.1 mol/L, 100 μL) was added to the frozen tissue and homogenized for 1.5 min at 20 Hz (Tissuelyser II, Qiagen, Germany). Ice-cold 60% ethanol (800 μL) was further added and the mixture homogenized again, before centrifugation at 14,000 g for 10 min. The supernatant was then collected. The extraction steps were repeated twice with 800 μL 60% ethanol to extract the metabolites remaining in the sediment. All the supernatants were collected and desiccated in a centrifugal drying apparatus (Thermo Scientific 2010, Germany) and freezing vacuum dryer (Thermo Scientific).

The dried product was preserved for further NMR studies. The dried product was successively dissolved in 60 μL D_2O (containing the inner standard, 3-(trimethylsilyl) propionic-2, 2, 3, 3-d_4 acid sodium salt (TSP, 120 mg/ L; 269913-1G, Sigma-Aldrich)) and 540 μL phosphate buffer (pH 7.2). The solution was mixed in a high-speed vortex and centrifuged at 14,000 g for 15 min, and the supernatant was withdrawn and transferred to an NMR tube.

Acquisition of PMRS

PMRS spectra were acquired as in previous studies [1, 2]. The extracted samples were measured with a Bruker Avance III 600 MHz NMR spectrometer (298 K) equipped with an inverse cryogenic probe (Bruker BioSpin, Germany). The spectra were acquired with a standard Watergate pulse sequence [3]. The following acquisition parameters were set for every sample: p1 (90 °C pulse), 8.35 μs; number of scans, 256; spectral width, 20 ppm; dummy scans, 8; number of free-induction decay points, 32 K.

PMRS data processing

All PMRS were processed and analyzed with TopSpin (Version 2.1, Bruker BioSpin) and a home-made software NMRSpec [4]. First, the phase correction and baseline distortion were manually completed in TopSpin. Then the corrected spectra were imported into NMRSpec for spectrum alignment, peak extraction, spectral integration, and the integration of chemical-related peaks. This software has been used in several metabolomics studies [1, 5, 6]. The chemical shifts of major amino-acids were distributed in the range of 1.20–4.46 ppm, so this gap was extracted for further analysis. First of all, the areas of all peaks (area under the curve) in this gap were automatically calculated for further statistical analysis [1]. To compensate for the different concentrations, each peak area was normalized to the sum of all the peak areas in this gap of its own spectrum prior to the discriminant analysis [2, 7, 8]. Furthermore, the absolute concentrations (lmol/g wet weight) of the identified metabolites were calculated with the related peak areas in spectra from the samples, information on the internal standards (TSP, such as concentration and proton number), and specimen weight. The calculation was as follows:

$$C_{met} = \frac{A_{met} / (R_{met} * N_H)}{A_{TMSP}} * (C_{TMSP} * V_{TMSP}) * 9/Wt$$

where Amet and ATSP are the relative areas of the peaks of the detected metabolites and TSP, and R_{met} is a constant for a specific metabolite calculated as the ratio between the partial NMR signal of the standard metabolite in selected regions (almost pure chemical signal) in a real sample and the whole proton signal in the standard spectrum; NH is the number of protons of the metabolite within the area A_{met}; C_{TSP} and V_{TSP} are the concentration and volume of TSP standard solution added to the NMR tube; *Wt* is the total weight of the wet specimen and 9 is the number of protons in the TSP.

Supplementary References

1. Liu T, He Z, Tian X, Kamal GM, Li Z, Liu Z, Liu H, Xu F, Wang J, Xiang H. Specific patterns of spinal metabolites underlying α-Me-5-HT-evoked pruritus compared with histamine and capsaicin assessed by proton nuclear magnetic resonance spectroscopy. Biochim Biophys Acta Mol Basis Dis. 2017; 1863:1222–30. https://doi.org/10.1016/j.bbadis.2017.03.011 PMID:28344131

2. Du H, Fu J, Wang S, Liu H, Zeng Y, Yang J, Xiong S. 1H-NMR metabolomics analysis of nutritional components from two kinds of freshwater fish brain extracts. RSC Advances. 2018; 8:19470–78. https://doi.org/10.1039/C8RA02311E

3. Liu ML, Mao XA, Ye CH, Huang H, Nicholson JK, Lindon JC. Improved WATERGATE pulse sequences for solvent suppression in NMR spectroscopy. J Magn Reson. 1998; 132:125–29. https://doi.org/10.1006/jmre.1998.1405

4. Liu Y, Cheng J, Liu HL, Deng YH, Wang J, Xu FQ. NMRSpec: an integrated software package for processing and analyzing one dimensional nuclear magnetic resonance spectra. Chemom Intell Lab Syst. 2017; 162:142–48. https://doi.org/10.1016/j.chemolab.2017.01.005

5. Kamal GM, Wang X, Bin Yuan, Wang J, Sun P, Zhang X, Liu M. Compositional differences among Chinese soy sauce types studied by (13)C NMR spectroscopy coupled with multivariate statistical analysis. Talanta. 2016; 158:89–99. https://doi.org/10.1016/j.talanta.2016.05.033 PMID:27343582

6. Kamal GM, Yuan B, Hussain AI, Wang J, Jiang B, Zhang X, Liu M. (13)C-NMR-Based Metabolomic Profiling of Typical Asian Soy Sauces. Molecules. 2016; 21:1168. https://doi.org/10.3390/molecules21091168 PMID:27598115

7. Wang J, Zeng HL, Du H, Liu Z, Cheng J, Liu T, Hu T, Kamal GM, Li X, Liu H, Xu F. Evaluation of metabolites extraction strategies for identifying different brain regions and their relationship with alcohol preference and gender difference using NMR metabolomics. Talanta. 2018; 179:369–76. https://doi.org/10.1016/j.talanta.2017.11.045 PMID:29310246

8. Zhang L, Wang L, Hu Y, Liu Z, Tian Y, Wu X, Zhao Y, Tang H, Chen C, Wang Y. Selective metabolic effects of gold nanorods on normal and cancer cells and their application in anticancer drug screening. Biomaterials. 2013; 34:7117–26. https://doi.org/10.1016/j.biomaterials.2013.05.043 PMID:23787109

Supplementary Figures

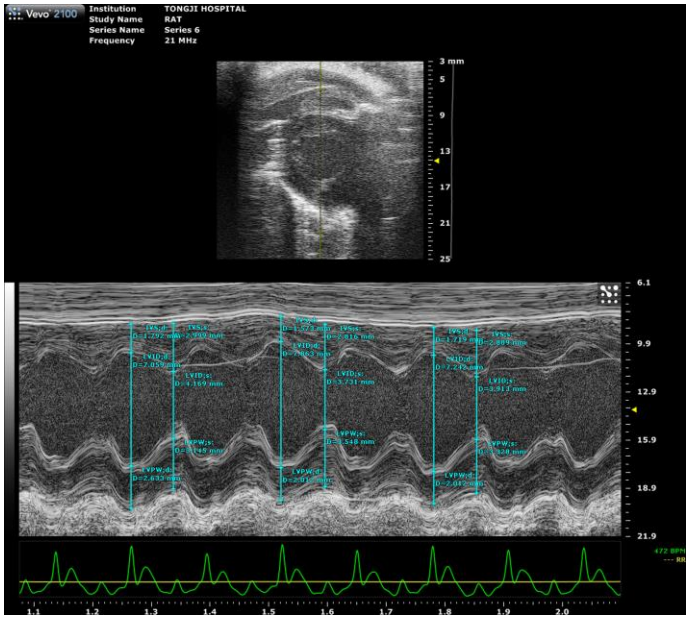

Supplementary Figure 1. Cardiac function assessed by M-mode echocardiograms in the Control group. For echocardiographic analyses, images were recorded in parasternal long-axis projections with guided one-dimensional M-mode recordings at the mid ventricular level. Standard measurements of inter-ventricular septum (IVS), left ventricular internal diameter (LVID) and left ventricular posterior wall (LVPW) were performed in systole and diastole in parasternal long-axis projection.

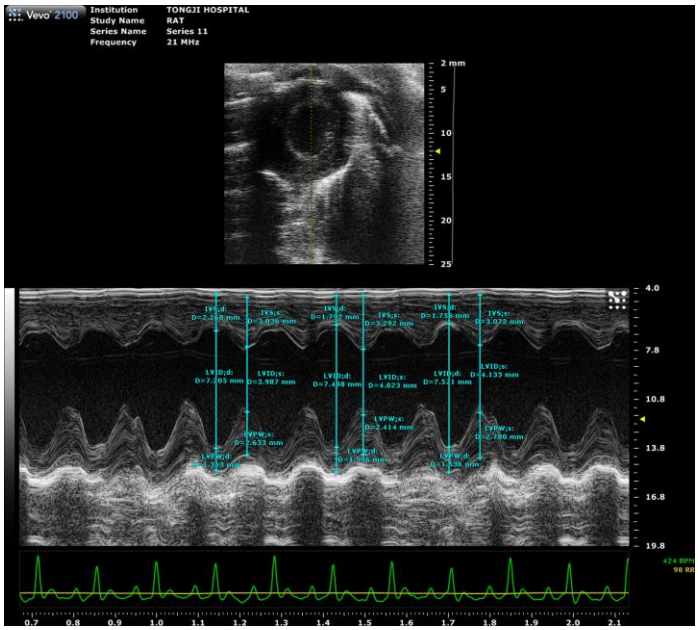

Supplementary Figure 2. Cardiac function assessed by M-mode echocardiograms in the IR group. For echocardiographic analyses, images were recorded in parasternal long-axis projections with guided one-dimensional M-mode recordings at the mid ventricular level. Standard measurements of inter-ventricular septum (IVS), left ventricular internal diameter (LVID) and left ventricular posterior wall (LVPW) were performed in systole and diastole in parasternal long-axis projection.

Supplementary Tables

Please browse Full Text version to see the data of Supplementary Table 2.

Supplementary Table 1. LVEF(%) and LVFS(%) of two groups 2h after MIRI.

	Baseline	MIRI 2h
LVEF(%)		
Con Group	72.42 ± 3.193	69.94 ± 2.478
IR Group	75.49 ± 1.512	65.65 ± 2.478*
LVFS(%)		
Con Group	42.15 ± 2.878	38.81 ± 2.849
IR Group	43.31 ± 1.077	34.16 ± 1.353**

Averaged data ejection fraction (LVEF) and fractional shortening (LVFS) assessed by echocardiography in male SD rats subjected to control or IR injury (30 min ischemia and 2h reperfusion). n = 4 rats per group. Results were expressed as mean ± SEM, *P < 0.01, **P < 0.001. Student's t-test as compared to Con group basal state.

Supplementary Table 2. The level of metabolites in 12 brain regions of two groups.